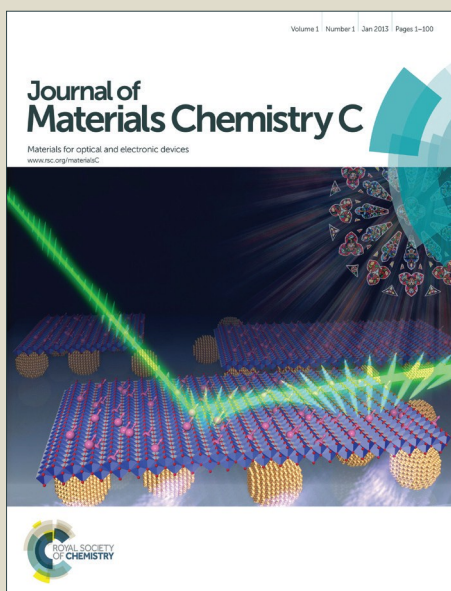


Journal of Materials Chemistry C

Accepted Manuscript



This is an *Accepted Manuscript*, which has been through the Royal Society of Chemistry peer review process and has been accepted for publication.

Accepted Manuscripts are published online shortly after acceptance, before technical editing, formatting and proof reading. Using this free service, authors can make their results available to the community, in citable form, before we publish the edited article. We will replace this *Accepted Manuscript* with the edited and formatted *Advance Article* as soon as it is available.

You can find more information about *Accepted Manuscripts* in the [Information for Authors](#).

Please note that technical editing may introduce minor changes to the text and/or graphics, which may alter content. The journal's standard [Terms & Conditions](#) and the [Ethical guidelines](#) still apply. In no event shall the Royal Society of Chemistry be held responsible for any errors or omissions in this *Accepted Manuscript* or any consequences arising from the use of any information it contains.



Journal Name

ARTICLE

An organic-metal-inorganic three-component nanojunction array: design, construction and its reversible diode-like resistive electrical switching behavior

Received 00th January 20xx,
Accepted 00th January 20xx

DOI: 10.1039/x0xx00000x

www.rsc.org/

Jing Wang^a, Weiqing Xu^a, Xiangyuan Liu^{a,c}, Fou Bai^b, Xianghua Zhou^a, Shuping Xu^{a*}

A reversible diode-like resistive electrical switching composite material, AgTCNQF₄-AgNPs-TiO₂ organic-metal-inorganic hetero-nanojunction array, has been successfully prepared on a fluorine-doped tin oxide (FTO) glass slide. These AgTCNQF₄-AgNPs-TiO₂ nanojunctions shows obvious absorption bands in the visible to near-infrared region, which are assigned to the interfacial charge transfer from the TiO₂ to the AgTCNQF₄. Moreover, the local electrical properties of these AgTCNQF₄-AgNPs-TiO₂ nanojunctions have been tested in a device configuration of Au-tip/AgTCNQF₄-AgNPs-TiO₂/FTO and the measured results reveal that these AgTCNQF₄-AgNPs-TiO₂ nanojunctions possess many applicable functions involving the switchable diode effect, the reversible electrical switching and memory behaviors.

1. Introduction.

As one of important modern electronic and optoelectronic device configurations, hetero-nanojunctions have received great attentions and they have been widely utilized as most electronic and optoelectronic device components, such as light-emitting diodes,^[1-6] lasers,^[7,8] photovoltaic cells photodetectors, field-effect transistors.^[9-14] Compared with simplex semiconductor component devices in which the optoelectronics-related factors (e.g. crystallization, doping and alignment) have been well studied, hetero-nanojunctions show diversity in components and support more complex and coupled electronic states, which allow for a more logical device model and a better electronic and optoelectronic property.^[15-20] Based on this expectation, the hetero-nanojunction structure experiences from two components to three, even multi-components. Multi-component nanojunctions possess multiple active ingredients and spatial integrated electron transfer, which can meet high requirements on their behaviours. Metal-Organic charge-transfer complexes of MTCNQ and MTCNQF₄ (M = Cu or Ag; TCNQ = 7,7,8,8-tetracyanoquinodimethane and TCNQF₄ = 2,3,5,6-tetrafluoro-7,7,8,8-tetracyanoquinodimethane) have been applied to construct the optical and electrical memory devices,^[21-23] electrical switching^[24] and field emission transistors,^[25-27] owing to their memory effects, optical and electrical bistable behaviours.^[28-30] Compared with simplex semiconductor component devices, the multi-components

nanocomposite composed of MTCNQ(F₄) show diversity in components and have been extended to more application fields. For instance, the MTCNQ(F₄) micro-nanostructures combined with metal nanoparticles (MNPs) (M = Au, Ag, Pt, Pd, or Rh) are good catalysts and support charge transfer property.^[31-35] AgTCNQ and CuTCNQ nanowires grown on the large-area reduced graphene oxide (rGO/metal-TCNQ hybrid films) exhibited substantial photoconductivity, highly reproducible photoswitching^[36] and electronic switching behaviours.^[37] The metal oxide (ZnO) and CuTCNQ hybrid nanowire arrays could stabilize the organic field emitters and improve the field emission properties.^[38] Besides, ZnO/CuTCNQ as inorganic-organic p-n hierarchical nanostructures presented a fast-response/-recovery diode-type humidity sensor.^[39]

As one of ideal candidates in the electrical and optical switches, memory effects and field-emission properties,^[27,29,30] AgTCNQF₄ and its semiconductor properties are always hot topics. However, the combination of AgTCNQF₄ as a building block with other materials, e.g. inorganic semiconductors and metal nanoparticles,^[34,35] is still lacking. Herein, we designed and constructed a novel organic-metal-inorganic three-component nanojunction by the architecture of three kinds of nanostructures: AgTCNQF₄ nanorods (NRs), Ag nanoparticles (AgNPs) and TiO₂ NRs, and further developed a device of Au-tip/AgTCNQF₄-AgNPs-TiO₂/FTO. TiO₂ is a typical inorganic semiconductor, which has been extensively researched on their optical, and electrical properties.^[40] A vertically aligned TiO₂ NR array (60 ~ 222 nm in diameter and ~2.2 μm in length) was first prepared by using the hydrothermal method,^[41, 42] with the surface decoration of AgNPs (25 ~ 70 nm) by the photochemical growth^[43] and the top decoration of an urchin-like AgTCNQF₄ NR bunch (30 ~75 nm in diameter and 150 ~ 445 nm in length each) in the solution process.^[22] Through the analysis of the scanning electron microscopy (SEM), elemental energy-dispersive X-ray photoelectron spectroscopy (EDS), X-ray photoelectron spectroscopy (XPS), and ultraviolet-visible spectroscopy (UV-vis), we investigated the

^a State Key Laboratory of Supramolecular Structure and Materials, Institute of Theoretical Chemistry, Jilin University, Changchun 130012, P. R. China. *E-mail: xusp@jlu.edu.cn; Tel: +86-431-85168505.

^b College of Chemistry, Jilin University, Changchun 130012, P. R. China.

^c Department of Physics, School of Science, Changchun University of Science and Technology, Changchun 130022, P. R. China

†Electronic Supplementary Information (ESI) available. See DOI: 10.1039/x0xx00000x

morphology, the elemental composition and the crystal structure of the AgTCNQF₄-AgNPs-TiO₂ nanojunction array detailedly in comparison with the TiO₂ NR array and the AgNPs-TiO₂ NR array. The current-voltage (I-V) curves were measured using a self-made semiconductor characterization system (see Figure S1) and a conductive-atomic force microscope. A reversible diode-like resistive electrical switching property and a memory behaviour in the AgTCNQF₄-AgNPs-TiO₂ organic-metal-inorganic nanojunction array were revealed and discussed in present study.

2. Experimental.

2.1 Synthesis of AgTCNQF₄-AgNPs-TiO₂ Three-Component Nanojunction.

2.1.1 Synthesis of TiO₂ nanorod array. The TiO₂ NR array (1×3 cm²) was prepared through hydrothermal synthesis method (Scheme 1).^[41,42] The FTO coated glass (1 cm × 4 cm) initially cleaned by sonication in a mixed solution (isopropanol: acetone : ultrapure water is 1:1:1) for 60 min. 6.0 mL of ultrapure water and 6.0 mL of hydrochloric acid were mixed into a 25.0 mL Teflon-liner steel autoclave under stirring for 5 min. Then 1.0 mL of tetrabutyl orthotitanate was added into above mixture and the mixture was continued to stir for another 5 min. The FTO glass slides were placed aslant in above Teflon-liner. The reaction kettle was sealed and the hydrothermal synthesis was conducted at 150 °C for 3.5 h. The FTO slides were decorated with TiO₂ NR array and they removed from the kettle, cleaned by ultrapure water and dried in the air.

2.1.2 Synthesis of AgNPs-TiO₂ composite nanorod array. The AgNPs on the surface of TiO₂ NR array were prepared based on a photochemical *in situ* synthesis method (Scheme 1).^[43] Silver nitrate and trisodium in a proportion of 1:1 were mixed in water to prepare a total of 20 mL mixed solution (1 mM). The FTO slides with the TiO₂ NR array were immersed in above mixed solution. A 354 nm ultraviolet (UV) light lamp was used to irradiate the slides for 30 minutes. Under the UV light, TiO₂ NR array slowly changed its color from white to brown, indicating the formation of Ag NPs. These Ag

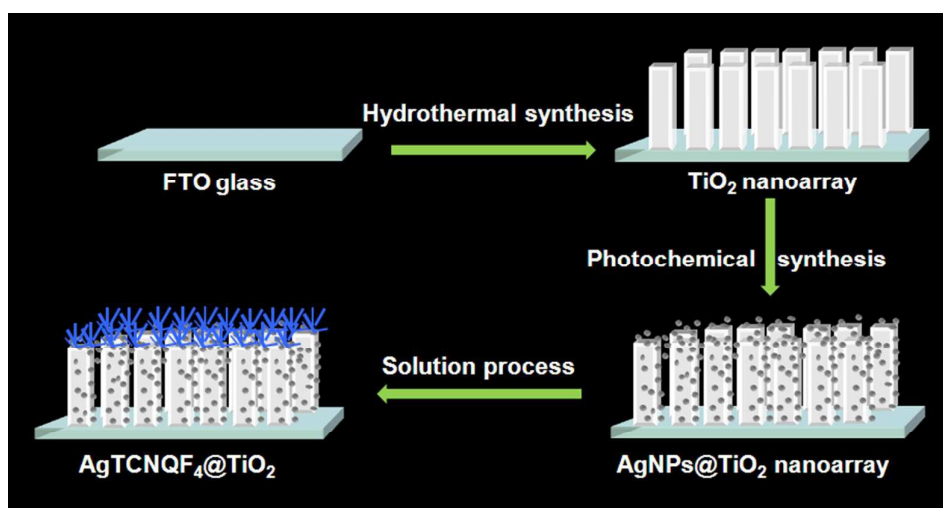
NPs over the TiO₂ array allow for AgTCNQF₄ NR bunch growing in the next step.

2.1.3 Synthesis of AgTCNQF₄-AgNPs-TiO₂ three-component nanojunction. The AgTCNQF₄ were produced on the AgNPs-TiO₂ arrays *via* the solution process (Scheme 1).^[22] The pre-synthesis AgNPs-TiO₂ composite NR array was slid into a TCNQF₄ acetonitrile solution (2.0 mg/mL) at room temperature for two minutes. After that, branches of AgTCNQF₄ crystals would form on the top of TiO₂ NR array.

In order to evaluate the electrical property of this three-component junction, we also constructed the AgTCNQF₄ microrods/Ag film and the AgTCNQF₄ microrods/FTO devices for comparison. Detailed descriptions about these two samples are provided in support information.

2.2 Instruments.

The morphologies of the TiO₂, AgNPs-TiO₂, AgTCNQF₄-AgNPs-TiO₂ were examined *via* a Hitachi SU8020 SEM and a JEM-2100F field emission TEM. The EDS was carried out on the Hitachi SU8020 scanning electronic microscope with a Bruker X-ray energy dispersive spectrometer, and an accelerating voltage of 20 kV. The XPS were implemented using an electron spectrometer (VG ESCALAB MK II). The Raman spectra were recorded from a Raman microscope system (Horiba-Jobin Yvon France) equipped with a 633 nm He-Ne ion laser and a water cooled charge-coupled device detector. The UV-vis absorption spectra were recorded with an Ocean Optics USB4000 spectrometer. The electrical property measurements were carried out using a self-made semiconductor characterization system (see Figure 4A and Figure S1). A Keithley sourcemeter (Model 2611) was used for recording I-V data, which is controlled by the Lab Tracer 2.0 software and connected with the photoelectric testing platform. We also employed a SPA300HV C-AFM (Seiko, Japan) for electrical characterization. The mode settings is "2ch.simul scan" mode with the parameters involving Area/Speed of 2000 nm/1 Hz, Force Ref of -0.5, Integral and Proportional gains of 0.4 and 0.2, respectively. The sample was fixed on a metal disk with the conductive copper pasted to ensure electrical contact. Au decorated Si tips (radius < 25 nm) were purchased from Budget Sensors.



Scheme 1. The strategy for preparing the AgTCNQF₄-AgNPs-TiO₂ three-component nanojunctions.

3. Results and discussion.

3.1 Design of hetero-nanojunctions

This organic-metal-inorganic three-component nanojunction was designed by the architecture of AgTCNQF₄ NRs, AgNPs and TiO₂ NRs, and further a device composed of Au-tip/AgTCNQF₄-AgNPs-TiO₂/FTO was built. As shown in Scheme 2, in this three-component nanojunction, AgNPs serve as an electron anti-blocking layer due to its work function of 4.26 eV, which bridge the Fermi-level of TiO₂ layer (rutile single crystals TiO₂ has the band gap (*E_g*) of 3.03 eV and the electron affinity of 4.8 eV^[43]) and AgTCNQF₄ layer (a work function of 1.07 eV^[27,34]). When AgTCNQF₄, AgNPs and TiO₂ are in order joined, an internal electric field will generate from AgTCNQF₄ to AgNPs, and next to TiO₂ (Scheme 2B). Meanwhile, the work function of Au is about 5.3 eV, which is lower than the Fermi level of AgTCNQF₄. When the Au tip touches AgTCNQF₄, a reversed internal electric field from AgTCNQF₄ to Au will be built at the Au-tip /AgTCNQF₄ interface (Scheme 2A). So, the device of Au-tip/AgTCNQF₄-AgNPs-TiO₂/FTO supports two heterojunction structures. Therefore, a reversible internal electric field in this three nanojunctions will be observed and a reversible electrical switching feature will be expected.

3.2 Characterization of AgTCNQF₄-AgNPs-TiO₂.

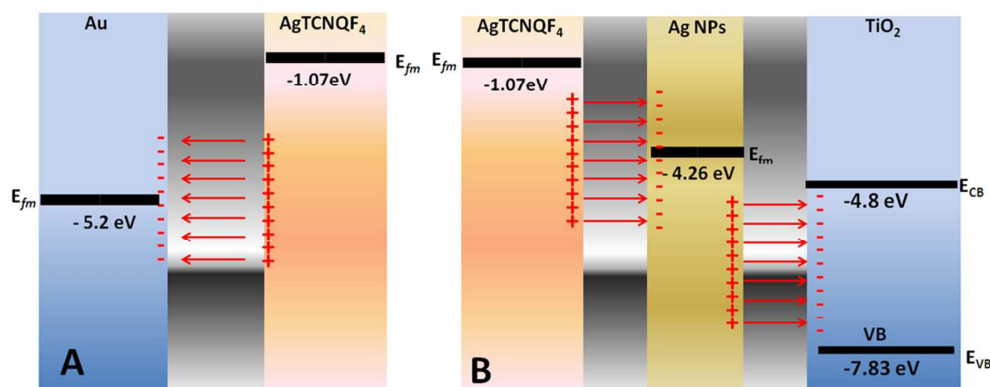
Figure 1A and 1B show the top view and cross sectional SEM images of the TiO₂ NR array grown on the FTO slide. The TiO₂ NR array was vertically aligned above the FTO slide. The average diameter and length of each TiO₂ NR are about 60 ~ 222 nm and 2.2 μm, respectively. Figure 1C and 1D show the top view and cross sectional SEM images of the AgNPs deposited TiO₂ NRs. A great number of AgNPs are observed on the sidewalls and tops of the TiO₂ NRs with the size of 25 ~ 70 nm. The SEM images of the prepared three-component nanojunction array (AgTCNQF₄-AgNPs-TiO₂) are shown in Figure 1E and 1F, in which the branches of AgTCNQF₄ NRs like urchins have grown on the top of a single TiO₂ NR. The diameter and the length of AgTCNQF₄ are about 30 ~ 75 nm and 150 ~ 445 nm.

The size and morphology of AgTCNQF₄-AgNPs-TiO₂ nanojunction were further characterized by TEM. Figure 2A shows that the

diameter and the length of whole AgTCNQF₄-AgNPs-TiO₂ nanojunction are 1.4 and 3.6 μm, which are larger than the result of unmodified TiO₂ obtained by Figure 1 A and B. Insert in Figure 2B shows that the AgTCNQF₄ NRs exist on both the top and the side of a single TiO₂ NR and their length is 350 ~ 500 nm.

The elemental composition of the three-component AgTCNQF₄-AgNPs-TiO₂ nanojunctions was measured and quantitated *via* the EDX and XPS techniques. The EDX spectrum of the AgTCNQF₄-AgNPs-TiO₂ is shown in Figure 3A, revealing the presence of C, Ag, Ti, N and F. The quantified EDX data are inserted in Figure 3A, and the atomic fraction data present the ratio of Ag : N is more than 1 : 4 in the three-component nanojunction, implying that a certain amount of silver are in the forms of AgNPs and other ones are in the form of Ag⁺ that are coordinated with TCNQF₄⁻ (1:4).^[45] The Ag 3d XPS spectrum of the AgTCNQF₄-AgNPs-TiO₂ nanojunction (Figure 3B) further proves the existence of AgNPs.^[46] Also, we recorded the Raman spectra of the TiO₂ NR array and the AgTCNQF₄-AgNPs-TiO₂ nanojunction array, as shown in Figure 3C. The Raman bands of the TiO₂ NR array are located in 107, 241, 443 and 610 cm⁻¹ (Figure 3C-a), which feature the Raman-active modes of pure rutile TiO₂.^[47] In the Raman spectrum of AgTCNQF₄-AgNPs-TiO₂ nanojunction (Figure 3C-b), the Raman signs of TiO₂ and AgTCNQF₄ (2217, 2203, 1642, 1446, 1270, 874, 640 and 354 cm⁻¹)^[48] can be clearly identified.

Figure 3D show the UV-vis absorption spectra of TiO₂ NR array, AgNPs-TiO₂ and AgTCNQF₄-AgNPs-TiO₂ three-component nanojunctions. The absorption band of TiO₂ is located in the ultraviolet photoabsorption range of 300~400 nm^[49] (curve a in Figure 3D), which is assigned to the electron transition of TiO₂. When AgNPs have been deposited on the TiO₂ NR array, the photoabsorption ranges extend to the visible range (curve b in Figure 3D). The broadened band from 450 to 600 nm is attributed to the plasmonic absorption of AgNPs.^[49] After the AgTCNQF₄ have grown on the top of the AgNPs-TiO₂, the photoabsorption range covers the ultraviolet, visible and near-infrared wavelengths (curve c in Figure 3D). The strong absorption bands at 300-550 and 550-900 nm are assigned to AgTCNQF₄.^[29] The newborn absorption bands in the visible and near-infrared regions means that the charge transfer transition appears from the AgTCNQF₄ to the conduction band of TiO₂.



Scheme 2. Energy band and internal electric field diagrams of the Au-AgTCNQF₄ (A) and the AgTCNQF₄-AgNPs-TiO₂ (B) nanojunctions.

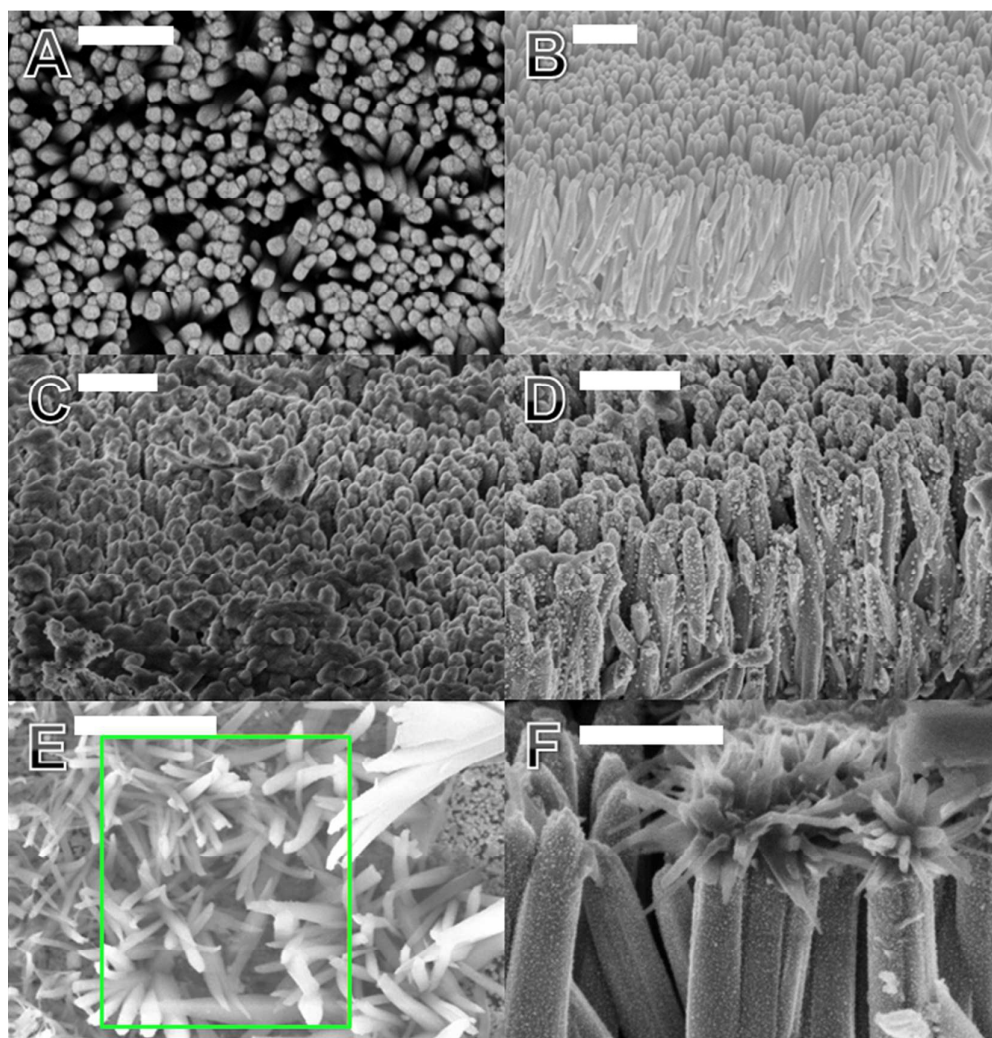


Figure 1. Top view and cross sectional SEM images of TiO_2 nanorod arrays (A and B), AgNPs-TiO_2 (C and D) and $\text{AgTCNQF}_4\text{-AgNPs-TiO}_2$ three-component nanojunction (E and F). The scales all are $1\ \mu\text{m}$.

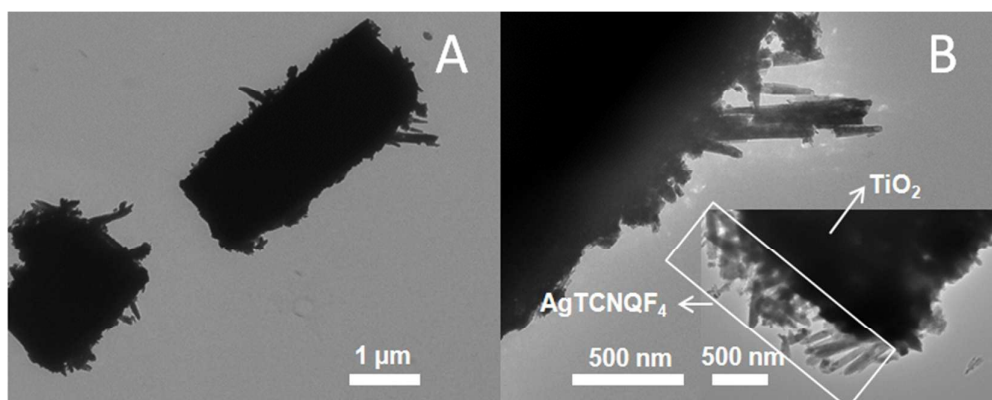


Figure 2. TEM images of the $\text{AgTCNQF}_4\text{-AgNPs-TiO}_2$ nanojunction under different magnifications.

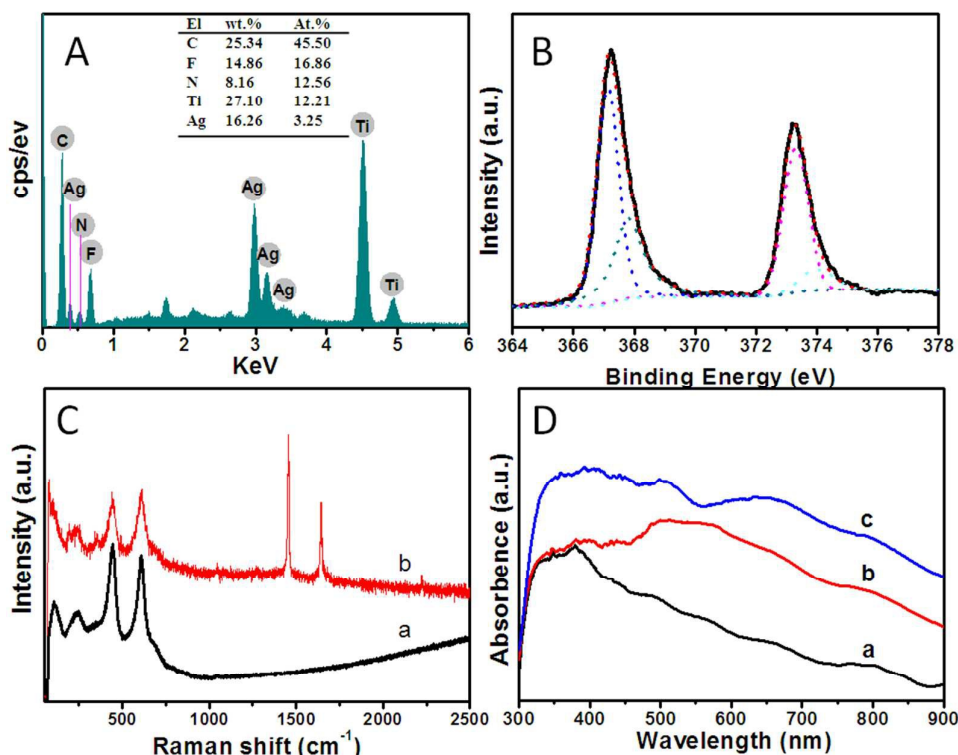


Figure 3. A) Energy-dispersive X-ray spectrum (EDS) of the AgTCNQF₄-AgNPs-TiO₂ three-component nanojunction. Insert is a table showing the percentages of elements. B) The Ag 3d XPS spectrum of the AgTCNQF₄-AgNPs-TiO₂ nanojunctions. C) The Raman spectra of the TiO₂ NRs (a) and the AgTCNQF₄-AgNPs-TiO₂ nanojunctions (b). D) The UV-vis absorption spectra of the TiO₂ NR array (a), AgNPs-TiO₂ array (b) and AgTCNQF₄-AgNPs-TiO₂ nanojunction array (c).

3.3 The local electrical properties of the devices.

The local electrical properties of these kinds of nanostructures in device configurations were investigated using a self-built semiconductor characterization system (Figure 4A), in which a positive voltage is applied to an Au coated tip as the top electrode (TE) and the FTO works as the bottom electrode (BE), while the FTO electrode remains at the ground level. The local current-voltage (*I-V*) of the devices of TiO₂/FTO(BE), AgNPs-TiO₂/FTO(BE), and AgTCNQF₄-AgNPs-TiO₂/FTO(BE) were measured at micrometric scale by attaching an Au tip (used as TE) to these devices, while the bidirectional sweeping voltages from + 5 to - 5 V (red curves) and from - 5 to + 5 V (green curves) were set.

The *I-V* curves of TiO₂ NR array (Figure 4B) show nonlinear and symmetric, revealing the semiconductor characteristic of TiO₂.^[50] Similarly, Under the action of negative voltage, the AgNPs-TiO₂ array (Figure 4C) shows similar *I-V* curves as the unmodified TiO₂ array. However, when the positive voltage applied to the AgNPs-TiO₂ system, the current intensity goes rising from zero point. This is because an electronic anti-blocking layer has formed at the interface of metal Ag and semiconductor. This phenomenon is in conformity with the bidirectional sweeping voltage. Interestingly, after the AgTCNQF₄ NRs have grown on the top of AgNPs-TiO₂ (Figure 4D), an asymmetric *I-V* curve can be observed and it displays a typical diode-like rectifying *I-V* characteristic, indicating a forward and reverse diode behaviour formed in the AgTCNQF₄-AgNPs-TiO₂ three-component nanojunctions.^[51] This convinces our above speculation that two heterojunctions (involving the Au/AgTCNQF₄ and the AgTCNQF₄/TiO₂) coexist in this ternary system.

To further learn the local electrical properties, the C-AFM was employed to measure the contact resistance at different locations of an AgTCNQF₄ nanobranched in this three component nanojunction. This characterization supports a high resolution to nanoscale. The topography, current mapping, and corresponds to *I-V* curves of nanojunctions are shown in Figure 5. Besides, the *I-V* curves of different locations of an AgTCNQF₄ nanobranched are shown in Figure S2. The electrical properties at different locations are almost similar and they both present a reversible diode-like resistive electrical switching behavior. The voltage range is in ± 5 V (Figure 4D) and the *I-V* curves are almost central symmetric without hysteresis. However, as the sweep voltage range is to ± 9 V, hysteresis phenomena can be observed (Figure 5C, D and Figure S2). As the bias voltage is reduced from 9 to 0 V, the *I-V* curves from a low resistance state ("LRS" or "ON") gradually reach zero point. When keeping backward scanning from 0 to - 9 V, at first, the *I-V* curve remains in the high resistance state ("HRS" or "OFF") till the bias voltage reaches - 4 V. And then, the *I-V* curve gradually increases, showing an "ON" state again. During the forward sweep from - 9 to 9 V, the *I-V* curve returns to zero with the bias voltage reaches zero point. Similarly, the curve remains in an "OFF" state till the bias voltage reaches 4V, following by the increase of the voltage and the recovery of the "on" state. As the bias voltage is reduced from 9 to 0 V, the *I-V* curve forms a low resistance state ("LRS" or "ON") and gradually reaches zero point. When keeping backward scanning from 0 to - 9 V, at first, the *I-V* curve remains in the high resistance state ("HRS" or "OFF") till the bias voltage reaches - 4 V. And then, the *I-V* curve gradually goes uprising, showing an "ON" state

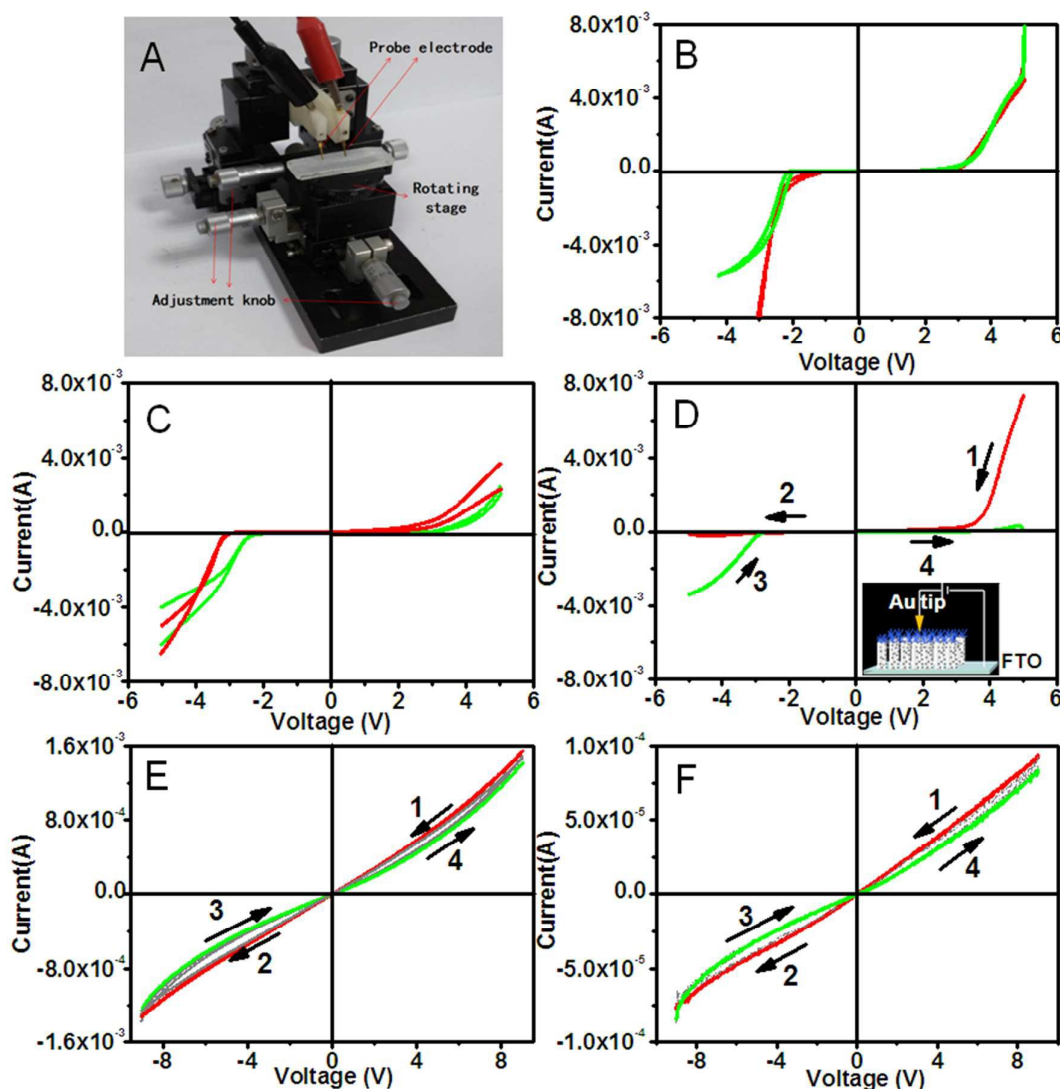


Figure 4 The picture of self-made semiconductor characterization system (A). The I - V curves of the Au-tip/ TiO_2 /FTO (B), Au-tip/AgNPs- TiO_2 /FTO(C), and Au-tip/AgTCNQF₄-AgNPs- TiO_2 /FTO(inset: the schematic diagram of measuring I - V curves)(D) Au-tip/AgTCNQF₄/FTO(E) and Au-tip/AgTCNQF₄/Ag film(F) measured in dark. The red curves were measured in a reverse sweep (from positive to negative voltages) while the green curves were measured in a forward sweep (from negative to positive voltages).

again. During the forward sweep from -9 to 9 V, the I - V curve returns to zero with the bias voltage reaches zero point. Similarly, the curve remains in an "OFF" state till the bias voltage reaches 4V, following by the increase of the voltage and the recovery of the "on" state.

In order to compare the electrical properties of AgTCNQF₄-AgNPs- TiO_2 nanojunction with traditional and single semiconductor component AgTCNQF₄ (synthetic method are supplied as support information), the reversible I - V curves were measured for the Au-tip/AgTCNQF₄/Ag film device and the Au-tip/AgTCNQF₄/FTO device, which are shown in Figure 4E and F, respectively. Besides the alike curves, Au-tip/AgTCNQF₄/FTO has a much higher forward current, which is up to 100 times than that of Au-tip/AgTCNQF₄/Ag film. The backward (red line) and forward (green line) I - V curves of AgTCNQF₄-AgNPs- TiO_2 three-component nanojunction are located at the upper and lower sides, respectively, and they intersect at

zero point, which is different from the one that the backward (red line) and forward (Green line) I - V curves of single semiconductor AgTCNQF₄ (Figure 4E and F), in which an "upside down" state at the crossing zero point is observed. To summary of the I - V curves, we can find the three-component nanojunction (AgTCNQF₄-AgNPs- TiO_2) and the single semiconductor component (AgTCNQF₄) have different resistive switching modes. The former configuration belongs to the reversible diode-like resistive electrical switching, while the latter one regards as the reversible resistive electrical switching.

The I - V curves of AgTCNQF₄-AgNPs- TiO_2 nanojunctions also exhibit close circles electrical switching property, which has been investigated by sweeping the bidirectional bias voltage on the devices. Figure 6A shows the local electrical switching I - V characteristics measured on the device Au-tip/AgTCNQF₄-AgNPs-

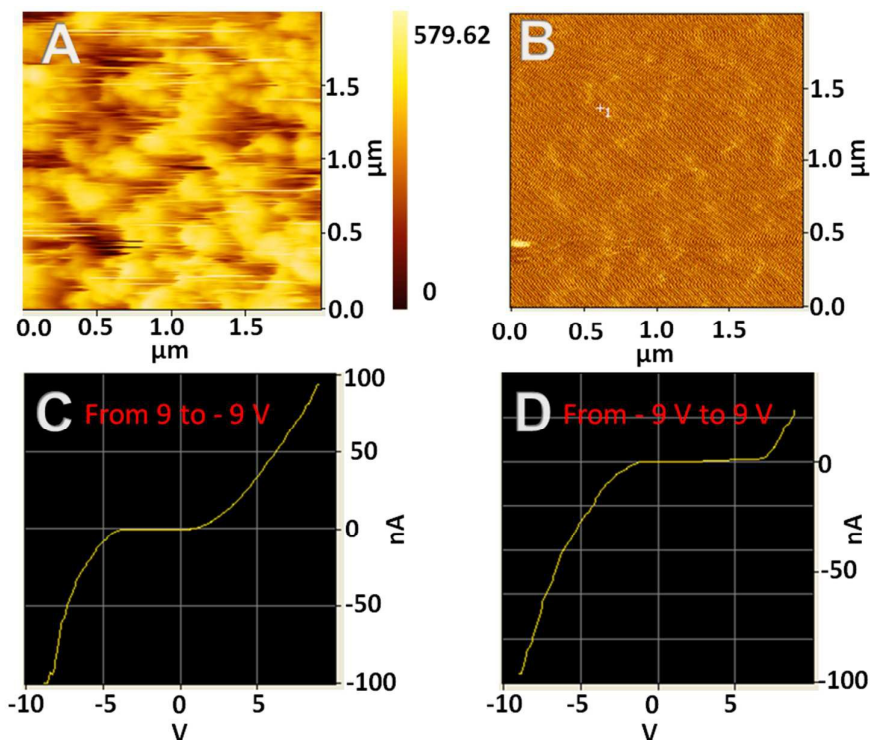


Figure 5. The topography image (A), current mapping (B) and corresponds to current-voltage (*I-V*) curves of AgTCNQF₄-AgNPs-TiO₂ three component nanojunction in the sign of “+1”, which were scanned by a conductive-atomic force microscope (C-AFM). The scanning voltage is from 9 to -9 V (C) and from -9 to 9 V (D).

TiO₂/FTO. The measurement was carried out with 4 cycles by sweeping the bias voltage of Au tip electrode from 9 to -9 V, followed by a reverse sweep from -9 to 9 V, repeatedly. It can be observed that both devices possess the obvious reversible resistive electrical switching behaviours. The *I-V* curves of Au-tip/AgTCNQF₄-AgNPs-TiO₂/FTO display the reversible hysteretic switching and memory behaviours. To further understand the resistive switching in AgTCNQF₄-AgNPs-TiO₂ nanojunctions, the Log *I* / *I* - *V* curves of the Au-tip/AgTCNQF₄-AgNPs-TiO₂/FTO (the sequences of voltage sweeps are marked as 1, 2, 3 and 4) and the Au-tip/AgTCNQF₄/Ag films (the sequences of voltage sweeps are marked as a, b, c and d) are plotted (Figure 6B). The resistive state of the three-component nanojunction shows the remaining HRS-LRS (or HRS-LRS) when reverse (or forward) sweeps across the zero voltage point is applied on, while the single component AgTCNQF₄ shows apparent LRS-LRS (or HRS-HRS) as the bias through the zero voltage. Therefore, we can deduce that the AgTCNQF₄-AgNPs-TiO₂ three-component nanojunction possesses the switchable diode effect.^[52] The *R*_{on}/*R*_{off} ratio of AgTCNQF₄-AgNPs-TiO₂ three-component nanojunction is up to 100 when the sweep voltage is set at 4V, which is much higher above that of AgTCNQF₄.

4. Conclusion

In summary, we designed and constructed an AgTCNQF₄-AgNPs-TiO₂ organic-metal-inorganic three-component nanojunction array and it shows a p-n junction between AgTCNQF₄ NRs and TiO₂ NRs. Electrical property measurements of the AgTCNQF₄-AgNPs-TiO₂

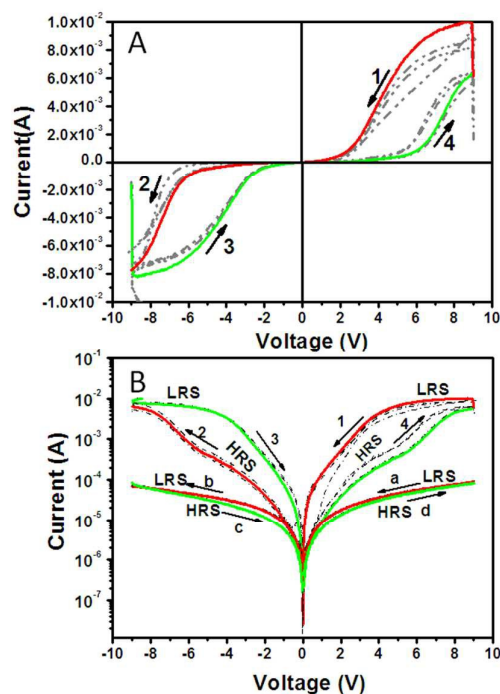


Figure 6. (A) The local switching *I-V* characteristics of the Au-tip/AgTCNQF₄-AgNPs-TiO₂/FTO. (B) The Log *I* / *I* - *V* characteristics of the Au-tip/AgTCNQF₄-AgNPs-TiO₂/FTO (the sequence of voltage sweeps are marked as 1, 2, 3 and 4) and the Au-tip/AgTCNQF₄/Ag films (the sequence of voltage sweeps are marked as a, b, c and d) in four circles. The red curves were measured in a reverse sweep (from positive to negative voltages), the green curves were measured in a forward sweep (from negative to positive voltages).

nanojunction display that AgTCNQF₄-AgNPs-TiO₂ possesses the reversible diode behaviour and the reversible diode-like resistive switching feature. The R_{ON}/R_{OFF} ratio of the AgTCNQF₄-AgNPs-TiO₂ nanojunctions is far away from the single component AgTCNQF₄, which makes it possible to be a three-component nanojunction memory device. Further study is still needed to accurately ascertain the mechanism of this reversible diode-like resistive switching behaviour in such an AgTCNQF₄-AgNPs-TiO₂ organic-metal-inorganic three-component nanojunction.

Acknowledgements

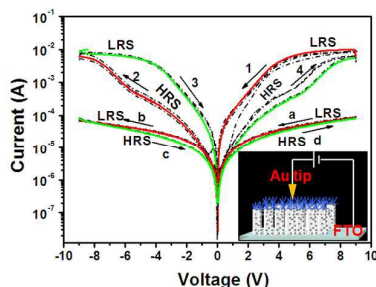
This work was supported by the National Instrumentation Program (NIP) of the Ministry of Science and Technology of China No. 2011YQ03012408, National Natural Science Foundation of China (91441105, 21373096, 21573087 and 21573092), and Science and Technology Development Program Funded Projects of Jilin province.

Notes and references

- [1] A. Tsukazaki, A. Ohtomo, T. Onuma, M. Ohtani, T. Makino, M. Sumiya, K. Ohtani, S. F. Chichibu, S. Fuke, Y. Segawa, H. Ohno, H. Koinuma, M. Kawasaki, *Nat. Mater.*, 2004, **4**, 42.
- [2] X. M. Zhang, M. Y. Lu, Y. Zhang, L. J. Chen, Z. L. Wang, *Adv. Mater.*, 2009, **21**, 2767.
- [3] M. C. Jeong, B. Y. Oh, M. H. Ham, S. W. Lee, J. M. Myoung, *Small*, 2007, **3**, 568.
- [4] R. Könenkamp, R. C. Word, M. Godinez, *Nano Lett.*, 2005, **5**, 2005.
- [5] X. B. Tang, G. M. Li, S. M. Zhou, *Nano Lett.*, 2013, **13**, 5046.
- [6] Y. B. Guo, Q. X. Tang, H. B. Liu, Y. J. Zhang, Y. L. Li, W. P. Hu, S. Wang, D. Zhu, *J. Am. Chem. Soc.*, 2008, **130**, 9198.
- [7] P. Petroff, R. L. Hartman, *J. Appl. Phys.*, 1974, **45**, 3899.
- [8] P. Petroff, R. L. Hartman, *Appl. Phys. Lett.*, 1973, **23**, 469.
- [9] T. Minura, S. Hiyamizu, T. Fujii, K. Nanbu, *Jpn. J. Appl. Phys.*, 1980, **19**, L225.
- [10] S. R. Puniredd, A. Kiersnowski, G. Battagliarin, W. Zajaczkowski, W. W. H. Wong, N. Kirby, K. Müllen, W. Pisula, *J. Mater. Chem. C*, 2013, **1**, 2433.
- [11] E. Wang, W. Mammo, M. R. Andersson, *Adv. Mater.*, 2014, **26**, 1801.
- [12] H. B. Liu, J. L. Xu, Y. J. Li, Y. L. Li, *Acc. Chem. Res.*, 2010, **43**, 1496.
- [13] Y. B. Guo, L. Xu, H. B. Liu, Y. J. Li, C. M. Che, Y. L. Li, *Adv. Mater.*, 2015, **27**, 985.
- [14] H. Y. Zheng, Y. J. Li, H. B. Liu, X. D. Yin, Y. L. Li, *Chem. Soc. Rev.*, 2011, **40**, 4506.
- [15] H. Tada, T. Mitsui, T. Kiyonaga, T. Akita, K. Tanaka, *Nat. Mater.*, 2006, **5**, 782.
- [16] L. S. Zhang, K. H. Wong, Z. G. Chen, J. C. Yu, J. C. Zhao, C. Hu, C. Y. Chan, P. K. Wong, *Appl. Catal. A*, 2009, **363**, 221.
- [17] C. Hu, Y. Q. Lan, J. H. Qu, X. X. Hu, A. M. Wang, *J. Phys. Chem. B*, 2006, **110**, 4066.
- [18] Y. Hou, X. Y. Li, Q. D. Zhao, X. Quan, G. H. Chen, *J. Mater. Chem.*, 2011, **21**, 18067.
- [19] F. Dong, H. Q. Wang, G. Sen, Z. B. Wu, S. C. Leed, *J. Hazardous Mater.*, 2011, **187**, 509.
- [20] H. M. Zhu, B. F. Yang, J. Xu, Z. P. Fu, M. W. Wen, T. Guo, S. Q. Fu, J. Zuo, S. Y. Zhang, *Appl. Catal. B: Environ.*, 2009, **90**, 463.
- [21] J. C. Xiao, Z. Y. Yin, Y. C. Wu, J. Guo, Y. H. Cheng, H. Li, Y. Z. Huang, F. Boey, H. Zhang, Q. C. Zhang, *Small*, 2011, **7**, 1242.
- [22] B. Mukherjee, M. Mukherjee, J. Park, S. Pyo, *J. Phys. Chem. C*, 2010, **114**, 567.
- [23] C. Muller, D. Deleruyelle, R. Muller, M. Thomas, A. Demolliens, Ch. Turquat, S. Spiga, *Solid-State Electron.*, 2011, **56**, 168.
- [24] R. Müller, O. Rouault, A. Katzenmeyer, L. Goux, D. J. Wouters, J. Genoe, P. Heremans, *Philos. Trans. R. Soc. A*, 2009, **367**, 4191.
- [25] K. Xiao, J. Tao, Z. W. Pan, A. A. Puzetzy, I. N. Ivanov, S. J. Pennycook, D. B. Geohegan, *Angew. Chem.* 2007, **119**, 2704.
- [26] C. N. Ye, K. B. Zheng, W. L. You, G. R. Chen, *Nanoscale. Res. Lett.*, 2010, **5**, 1307.
- [27] C. B. Ouyang, Y. B. Guo, H. B. Liu, Y. J. Zhao, G. X. Li, Y. J. Li, Y. L. Song, Y. L. Li, *J. Phys. Chem. C*, 2009, **113**, 7044.
- [28] E. I. Kamitsos, W. M. Risen Jr, *Solid State Commun.*, 1983, **45**, 165.
- [29] A. M. Kotsiliou, W. M. Risen Jr, *Solid State Commun.*, 1988, **68**, 503.
- [30] R. S. Potember, T. O. Poehler, *Synth. Met.*, 1982, **4**, 371.
- [31] A. Pearson, A. P. O' Mullane, S. K. Bhargava, V. Bansal, *Inorg. Chem.*, 2012, **51**, 8791.
- [32] A. Pearson, A. P. O' Mullane, *ChemPlusChem*, 2013, **78**, 1343.
- [33] A. Pearson, V. Bansal, A. P. O' Mullane, *Electrochimica Acta*, 2013, **114**, 189.
- [34] J. Wang, W. Q. Xu, J. X. Wu, G. T. Yu, X. H. Zhou, S. P. Xu, *J. Mater. Chem. C*, 2014, **2**, 2010.
- [35] J. Wang, W. Q. Xu, J. J. Zhang, S. P. Xu, *J. Phys. Chem. C*, 2014, **118**, 24752.
- [36] S. Zhang, Z. F. Lu, L. Gu, L. L. Cai, X. B. Cao, *Nanotechnology*, 2013, **24**, 46520.
- [37] E. Nossol, A. B. S. Nossol, S. X. Guo, J. Zhang, X. Y. Fang, A. J. G. Zarbin, A. M. Bond, *J. Mater. Chem. C*, 2014, **2**, 870.
- [38] H. Liu, S. Cui, Y. Guo, Y. Li, C. Huang, Z. Zuo, X. Yin, Y. Song, D. Zhu, *J. Mater. Chem.*, 2009, **19**, 1031.
- [39] K. Wang, X. M. Qian, L. Zhang, Y. J. Li, H. B. Liu, *ACS Appl. Mater. Interf.*, 2013, **5**, 5825.
- [40] H. Tang, K. Prasad, R. Sanjinès, P. E. Schmid, F. Lévy, *J. Appl. Phys.*, 1994, **75**, 2042.
- [41] B. Liu, E. S. Aydil, *J. Am. Chem. Soc.*, 2009, **131**, 3985.
- [42] X. J. Feng, K. Shankar, O. K. Varghese, M. Paulose, T. J. Latempa, C. A. Grimes, *Nano Lett.*, 2008, **8**, 3781.
- [43] D. O. Scanlon, C. W. Dunnill, J. Buckeridge, S. A. Shevlin, A. J. Logsdail, S. M. Woodley, C. R. A. Catlow, M. J. Powell, R. G. Palgrave, I. P. Parkin, G. W. Watson, T. W. Keal, P. Sherwood, A. Walsh, A. A. Sokol, *Nature Materials*, 2013, **12**, 798.
- [44] D. W. Li, L. J. Pan, S. Li, K. Liu, S. F. Wu, W. Peng, *J. Phys. Chem. C*, 2013, **117**, 6861.
- [45] K. Xiao, M. N. Yoon, A. J. Rondinone, E. A. Payzant, D. B. Geohegan, *J. Am. Chem. Soc.*, 2012, **134**, 14353.
- [46] X. Yuan, T. J. Yeow, Q. B. Zhang, J. Y. Lee, J. P. Xie, *Inorg. Chem.*, 2009, **48**, 10697.
- [47] H. L. Ma, J. Y. Yang, Y. Dai, Y. B. Zhang, B. Lu, G. H. Ma, *Appl. Surf. Sci.*, 2007, **253**, 7497.
- [48] M. Meneghetti, C. Pecile, *J. Chem. Phys.*, 1986, **84**, 4149.
- [49] K. Awazu, M. Fujimaki, C. Rockstuhl, J. Tominaga, H. Murakami, Y. Ohki, N. Yoshida, T. Watanabe, *J. Am. Chem. Soc.*, 2008, **130**, 1676.
- [50] L. C. K. Liao, C. C. Lin, *Thin Solid Films*, 2008, **516**, 1998.
- [51] R. C. Wang, H. Y. Lina, *Sensor Actuat. B-Chem.*, 2010, **149**, 94.
- [52] F. Zhang, Y. B. Lin, H. Wu, Q. Miao, J. J. Gong, J. P. Chen, S. J. Wu, M. Zeng, X. S. Gao, J. M. Liu, *Chin. Phys. B*, 2014, **23**, 027702.

An organic-metal-inorganic three-component nanojunction array: design, construction and its reversible diode-like resistive electrical switching behavior

Jing Wang^a, Weiqing Xu^a, Xiangyuan Liu^{a,c}, Fou Bai^b, Xianghua Zhou^a, Shuping Xu^{a,*}



The AgTCNQF₄-AgNPs-TiO₂ as organic-metal-inorganic hetero-nanojunction shows switchable diode effect, the reversible electrical switching and memory behaviors.